INRAℰ

Annals of Forest Science

RESEARCH PAPER

Open Access

Check for updates

Estimation of aboveground biomass and carbon stocks of *Quercus ilex* L. saplings using UAV-derived RGB imagery

R. Juan-Ovejero[1,2,3] , A. Elghouat[3,4,5] , C. J. Navarro[4] , M. P. Reyes-Martín[3] , M. N. Jiménez[6] , F. B. Navarro[7] , D. Alcaraz-Segura[4,6,8*] and J. Castro[3]

Abstract

Key message Crown area, sapling height, and biovolume extracted from UAV-acquired RGB images provided accurate estimates of aboveground biomass and carbon stocks in a 5-year-old holm oak (*Quercus ilex* L.) plantation. Our models regressing UAV-derived sapling variables against ground-based measurements exhibited high R^2 values (0.78–0.89), thereby reflecting that RGB data can be used as an effective tool for measuring young individuals.

Context The monitoring of tree sapling performance from the early stages of reforestation is of particular importance in the context of the global efforts to restore forests. Yet, most models to estimate carbon sequestration are developed for adult trees. Thus, the few models specifically developed for young trees rely on ground-based field sampling of tree growth parameters, which is time-consuming and difficult to implement at large spatial scales.

Aims Our objectives were as follows: (1) to study the potential of UAV-based RGB imagery to detect and extract sapling variables (e.g., crown area, height, and biovolume) by comparing ground-based sapling measurements with UAV-derived data and (2) to compare the accuracy of the data estimated from RGB imagery with existing traditional field-based allometric equations.

Methods We used a 5-year-old holm oak (*Quercus ilex* L. subsp. *ballota* (Desf.) Samp.) plantation (*N* = 617 plants), and their crown area, height, and biovolume were estimated from RGB imagery. Subsequently, the plants were harvested and the UAV-derived data were compared with field-measured sapling height and aboveground biomass values. Carbon content in leaves and stems was measured in a subsample of the saplings to estimate carbon stocks.

Results The models fitted with UAV-derived variables displayed high performance, with R^2 values from 0.78 to 0.89 for height, leaf and stem biomass, total aboveground biomass, and carbon stocks. Moreover, aboveground biomass outputs calculated with field height and UAV-derived height using allometric equations exhibited R^2 values from 0.65 to 0.68.

Conclusions Given the affordable cost of RGB cameras and the versatility of drones, we suggest that UAV-based models may be a cost-effective method to estimate the biomass and carbon stocks of young plantations. However, further studies conducting drone flights in different conditions are needed to make this approach more scalable.

Keywords Allometric equations, Carbon sequestration, Early-stage tree plantations, RGB imagery, Sapling biomass, UAV-derived sapling variables

---

*Correspondence:
D. Alcaraz-Segura
dalcaraz@ugr.es
Full list of author information is available at the end of the article

1 Introduction

Anthropogenic carbon dioxide emissions are one of the major contributors to climate change (Lacis et al. 2010). Removing or reducing CO_2 content from the atmosphere is thus a critical component of climate policies in order to operationalize net-zero emissions targets (Fuss et al. 2020; Hansen et al. 2017). Trees store carbon during their growth at scales from centuries to millennia and are considered the most efficient, natural, and eco-friendly carbon absorbers (Turner-Skoff and Cavender 2019). In fact, it is estimated that the world's forests store around 363 Gt of carbon, sequestered both in above- and belowground live biomass, while additionally offering other valuable ecosystem services (Bellassen et al. 2011; Hu et al. 2022; Pan et al. 2011). Thus, carbon sequestration through forest recovery and restoration represents a priority for climate policymakers to avoid climate change's extreme consequences (Bastin et al. 2019; Lewis et al. 2019).

From local to global scales, estimating tree biomass and carbon accumulation is thus of paramount relevance to assess the potential of forest activities to act as carbon sinks (Keith et al. 2021; Weiskittel et al. 2015). However, implementing an integrated carbon accounting system remains challenging (Alivernini et al. 2016; Vacchiano et al. 2018). Monitoring restoration projects, naturally regenerated forests, and plantations with saplings (i.e., growing young trees of small size and slender stem) is essential to fully comprehend the mitigation benefit of forest ecosystems during their whole life cycles (Keith et al. 2021; Pan et al. 2022; van der Gaast et al. 2018). Moreover, this could help in implementing sustainable forest management practices in a climate-smart framework (IPCC 2022). Therefore, the development of rapid, inexpensive, and accurate methods for estimating and monitoring carbon sequestration by forests is of special relevance to address these challenges and assess their economic viability.

Traditional field-based methods for estimating biomass and carbon stocks have been widely used over the years since they provide accurate and detailed results. These methods either rely on a harvesting process in which different parts of the trees are cut, dried, and weighed or on field biometric measurements (i.e., diameter at breast height (DBH) and tree height) to establish allometric equations (e.g., Forrester et al. 2017; Sullivan et al. 2018; Vorster et al. 2020). High- and low-resolution satellite imagery, including data from optical and radar sensors, is also gaining relevance to estimate the aboveground biomass of mature forests (e.g., Li et al. 2020; Velázquez et al. 2022; Yang et al. 2020). However, field-based methods are time-consuming, labor-intensive, expensive, and limited in terms of spatial cover (Weiskittel et al. 2015), whereas the application of satellite data is limited by temporal and spatial resolution. Moreover, most studies using field-based methods or satellite images focus on adult trees and ignore seedlings and saplings, despite the need to estimate carbon stocks and monitor establishment success in artificially (i.e., reforestation and afforestation) and naturally regenerated forests in the frame of climate change mitigation, carbon credits, or global restoration commitments (Correia et al. 2018; Hall et al. 2006; Menéndez-Miguélez et al. 2021; Ruiz-Peinado et al. 2012; Sullivan et al. 2018). In fact, national or international policies of forest restoration for carbon sequestration usually require monitoring and auditing the development of trees from their early stages (REDD+; REDD 2010), making the abovementioned models inappropriate and less effective. Thus, the development of easy-to-use methods for sapling biomass measurements would be economically, environmentally, and ecologically beneficial and advantageous.

The use of drones or unmanned aerial vehicles (UAV) as data sources in environmental and ecological studies has gained interest in recent years (Anderson and Gaston 2013). UAVs have the ability to fly at low heights, and in various areas, even those difficult to access, which results in real-time high spatiotemporal resolution data (Ruwaimana et al. 2018). They are cost-effective, flexible, and safe and can reduce the data acquisition time compared to ground-based methods (Messinger et al. 2016; Murfitt et al. 2017). Different sensor types, including multispectral, hyperspectral, and light detection and ranging (LiDAR), have been evaluated with success to estimate the biomass and carbon stock of young trees and small plants (Abdullah et al. 2021; Edson and Wing 2011; Luo et al. 2017). However, the use of these sensors in drones is more expensive. RGB cameras, on the contrary, are less costly and require less processing while still providing high performance. For instance, Lussem et al. (2019) proposed an efficient method for monitoring grassland biomass by using color vegetation indices derived from a UAV-based RGB digital camera. Similarly, Navarro et al. (2020) and McCann et al. (2022) concluded that using RGB data coupled with the SFM (structure-from-motion photogrammetry) method is capable of estimating the aboveground biomass of mangrove ecosystems and individual shrub-sized plants, respectively, with high accuracy. However, UAV-mounted RGB has not yet been thoroughly evaluated for estimating the biomass and carbon stock of young plantations at the individual-sapling level, despite its potential to provide fast, scalable, and low-cost estimation.

The present study aimed to assess the biomass and carbon accumulated by young forest plantations by using a simple, inexpensive, and accurate approach based on point clouds derived from high-resolution RGB images.

Juan-Ovejero *et al. Annals of Forest Science*   (2023) 80:44

Page 3 of 14

Our specific objectives were as follows: (1) to investigate the potential of lightweight UAV RGB imagery to detect and extract sapling variables (i.e., crown area, height, and biovolume—volume of growing stock plus stem and leaves according to Schoene (2003)) at the individual level of young plantations by comparing ground-based sapling measurements with UAV-derived data and (2) to compare the accuracy of the data estimated from RGB imagery with existing traditional field-based allometric equations. Through this study, we seek to provide an approach that could be an effective and robust alternative to traditional ground-based methods for monitoring the carbon and biomass of early-stage tree plantations, even over large spatial scales.

2 Materials and methods

2.1 Study site and experimental setup

The study site was located at a Research Field Station of the Andalusian Institute of Agricultural and Fisheries Research and Training (IFAPA) (37°10′20.02″ N, 3°38′38.86″ W; Granada, southeastern Spain), a flat (slope ca. 2%), agricultural terrain at 625 m a.s.l. (Fig. 1).

The climate in the area is Mediterranean, characterized by hot, dry summers, mild winters, and with most of the rainfall occurring in autumn and spring. The mean annual rainfall is 389 mm, and the mean annual temperature is 15.3 °C, July being the warmest month with average temperatures of 25.9 °C and January the coldest one with 6.2 °C (period of 2006–2020, climatic data collected from a meteorological station located at IFAPA Research Field Station). The soil is classified as calcaric fluvisol with a clay loam texture (24.8% silt, 31.0% clay and 44.2% sand), a gravel content of 17.9%, pH value of 8.5, organic matter content of 1.20%, volumetric-soil-water content at wilting point of 11.36%, total C of 4.15%, and N content of 0.085% (analyses for a soil sample of the first 20 cm depth composed by five subsamples at different positions within the study site).

A randomized block design (five blocks with a surface of 56×28 m^2 separated 4 m from each other) was established in autumn 2017 at the study site (Fig. 1c). At each block, there were $28 \times 14 = 392$ sampling points separated 2 m from each other, occupied either by outplanted holm oak (*Quercus ilex* L. subsp. *ballota* (Desf.)
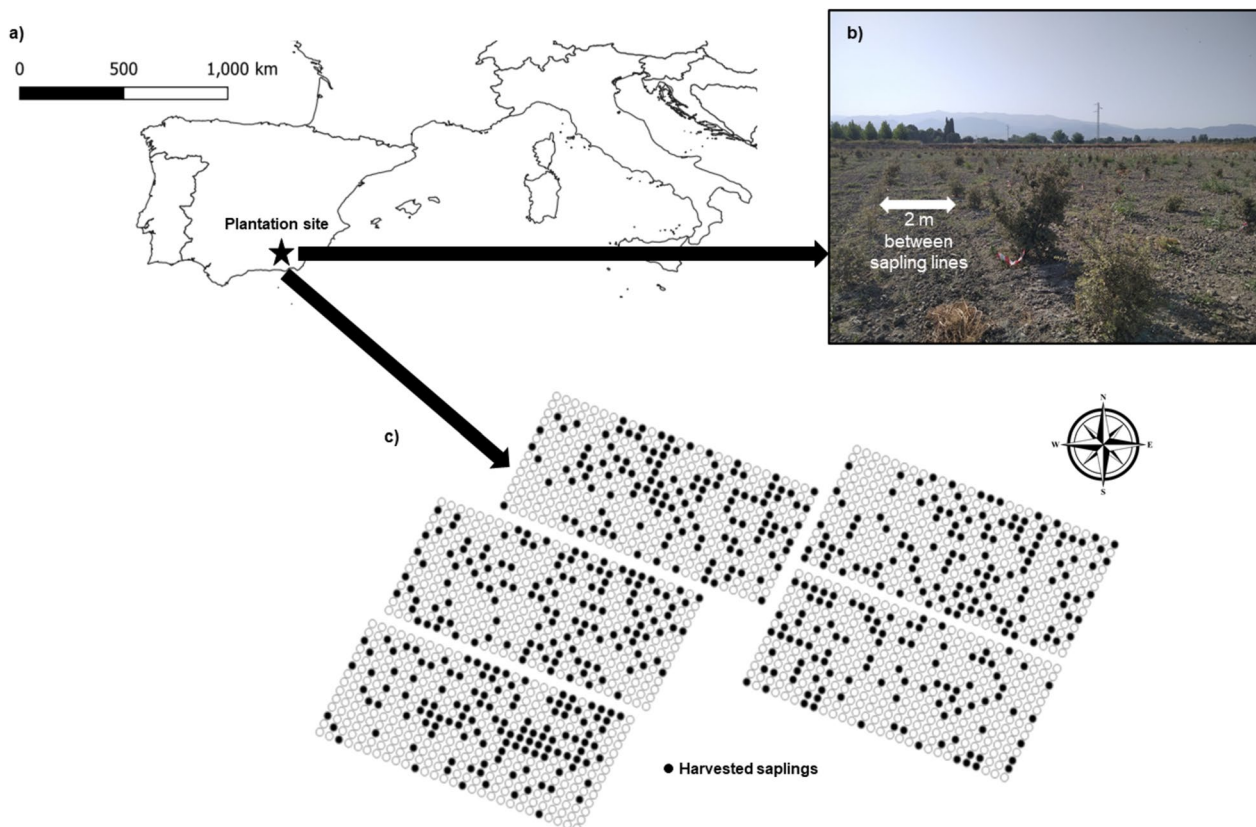

Fig. 1 Location of the study site (**a**), picture of the common garden experiment 4 years after outplanting (**b**), and location of the saplings that grew from the nursery-grown seedlings used in this study within the experimental setup (**c**). Each dot in **c** represents a position for a sapling (i.e., separated 2 m each other within each block), and black-colored dots are the nursery-grown saplings that were harvested for this study ($N = 617$)

Samp.) seedlings previously cultivated in a nursery or by holm oak seedlings from direct seeding. This design was planned within the context of an experiment about the effect of the reforestation method (planting *versus* direct seeding) on oak reforestation success. However, for the present study, we did not split our data along these blocks, and we only use data from the outplanted seedlings given that by the end of the experiment, they provided a higher number of plants from the same afforestation method and a greater range of plant sizes to test the objectives of the study.

Acorns were harvested in autumn 2016 and grown in a nursery using 45-alveoli forest trays with a capacity of 300 cm^3 per cell and commercial substrate (coconut coir dust and peat 50:50 enriched with controlled-release fertilizer (*15-9-11 + 2MgO + TE*; Osmocote®)). In December 2017, 899 nursery-grown seedlings were planted in the field site, evenly distributed among blocks in randomly selected sampling points (Fig. 1c). Seedling height and biomass (both above- and belowground) at the moment of outplanting were 25.73 ± 0.73 cm and 8.49 ± 0.24 g, respectively (average for 90 harvested nursery-grown seedlings). Plants were monitored in the field for 4 years, until September 2021. Thus, the number of plants monitored for the present study was 617 (Fig. 1c). To prevent herbaceous competition, weed removal was performed twice or three times (depending on the amount of rainfall) every year since the start of the experiment in December 2017 until autumn 2021. Weed removal was also carried out 1 week before the UAV flight.

2.2 Field measurements and carbon content analysis

Plant height and root collar diameter (two perpendicular measurements at the base of the trunk) were taken for all plants in mid-September 2021, when the UAV data was also acquired (see below). Afterwards, a harvest was performed between October and December 2021 by cutting the plants at the base of the trunk. All plants were oven-dried at 60 °C until constant weight, and leaves and stems were separated and weighted with a precision scale in grams to two decimal places to obtain leaf biomass, stem biomass, and total aboveground biomass measurements. A subsample of leaves was collected for 369 of the oven-dried plants to determine the leaf carbon content. Likewise, a stem subsection was extracted from 53 of these harvested individuals for stem carbon measurements. The carbon contents of the leaves and stems were measured in finely ground samples by means of a LECO elemental analyzer (LECO® TruSpec CN, St. Joseph, MI, USA) at the University of Granada (Spain). Leaf and stem carbon dry weights were calculated by multiplying each individual biomass measurement by the average values of leaf and stem % C, respectively. The total pool of carbon

was calculated for each plant by summing their estimates of leaf and stem carbon dry weights.

2.3 Crown area, sapling height, and biovolume estimations from UAV-based RGB imagery

A flight campaign with a Phantom 4 Advanced (DJI GMBH, Niederlauer, Germany) was conducted on September 17, 2021, using a Parrot Sequoia® (Parrot, Paris, France) high-resolution 20-megapixel RGB camera with a 4864 × 3648 pixel sensor (Figure 5 in Appendix). Aerial photographs were taken at a flight altitude of 40 m above the ground surface between 16:17 h and 17:04 h with sunny and cloudless meteorological conditions. To validate the UAV-derived height and volume estimates, 43 boxes of known shapes and sizes (ranging from 0.04 to 0.80 m in height and from 0.0009775 to 0.1152 m^3 in volume; Figure 5 in Appendix) were randomly laid on the ground at the common garden site before the flight. The volumes and heights measured in the laboratory and estimated by the UAV procedure were later statistically compared.

The UAV data were processed using Pix4Dmapper 4.7.5 (PIX4d, Lausanne, Switzerland). The data acquisition led to 589 images that were processed in five steps. First, the software automatically geolocated and matched 45,476 key common 2D tie points across multiple images. Second, a 3D dense point cloud was developed using the following settings: high point density, original image scale, and at least three image matches per 3D point. Third, each 3D point (297,959,814 in total) was automatically classified as bare ground, vegetation, or road and then manually verified or corrected by visually inspecting the 0.56 cm/pixel RGB orthomosaic image using the Pix4Dmapper editing tool. Fourth, all 3D points were used to generate the digital surface model (DSM) with a resolution of 0.57 cm/pixel, while only bare ground and road points were used to interpolate the digital terrain model (DTM) with a resolution of 2.86 cm/pixel. Finally, the canopy height model (CHM), which provides the plant height for each 0.57 cm pixel, was obtained by subtracting the DTM from the DSM in QGIS 3.12.3 (QGIS Development Team 2020).

To estimate the biovolume of each holm oak, pixels with CHM values greater than 10 cm (height of the smallest individual recorded in the field) were first polygonized to identify the crown area of each individual. This 10-cm threshold was used to clearly draw the contours of each plant and avoid confusions with any other types of soil coverage and meant that sapling height and biovolume of some very small plants could not be calculated. Hence, this resulted in a total sample size with available data for UAV estimates of 571.

For each polygon, we extracted two values, the pixel value with the maximum height, used as an estimator of

sapling height, and the sapling biovolume, which is the sum of the volumes of all pixels within each crown polygon, and the same procedure was followed with the boxes placed in the field for validation. The dataset containing all variables is available in Juan-Ovejero et al. (2023).

We therefore applied the following equation for sapling biovolume:

$$Biovolume(sapling) = \sum Volume(pixel) = Pixel\ width \times Pixel\ length \times Pixel\ height$$

where Pixel width = 0.56 cm and Pixel length = 0.56 cm

2.4 UAV-based RGB data versus existing traditional field-based allometric equations

To further evaluate the effectiveness of the RGB data, we used two allometric equations developed for young forest plantations. Specifically, we used our field and UAV-derived sapling height measurements to calculate total aboveground biomass with two generalized equations for a large group of forest tree species (1) and with a species-specific equation (2) (Menéndez-Miguélez et al. 2022):

$$Total\ aboveground\ biomass(evergreen\ broadleaves) = 0.7607\ (sapling\ height)^{2.7010} + \varepsilon' \tag{1}$$

$$Total\ aboveground\ biomass(Quercus\ ilex) = 0.6520(sapling\ height)^{2.8257} + \varepsilon' \tag{2}$$

where ε' is the residual term of the models.

2.5 Statistical analyses

We assessed significant correlations (p-value < 0.05) between field tree height and harvested aboveground biomass using Spearman correlation coefficients. We performed a linear regression with UAV-derived box measurements (i.e., box height and volume) against laboratory box measurements and extracted the values of the determination coefficient (R^2 adjusted; it provides an accurate measure of the goodness of fit of a model by considering the number of predictors and representing the proportion of the variance in the dependent variable explained by the independent variables), root-mean-square error (RMSE), and mean bias error (MBE). Additionally, we regressed variables estimated with drone data (i.e., maximum sapling height, biovolume, and crown area) against field height measurements, aboveground biomass, and aboveground carbon stocks and assessed their fits to different models (i.e., linear, polynomial of different orders, logarithmic, and inverse exponential). Among all obtained regression models, we ran model comparisons and selected those with the following: (1)

the highest R^2 adjusted, (2) the lowest RMSE and Akaike Information Criteria (AIC) values, and (3) the lowest number of terms in case the other two criteria were similar. Finally, the performance of RGB data was evaluated by comparing the total aboveground biomass outputs obtained from field and UAV-derived height using allometric equations and then regressing these outputs

against the real aboveground biomass values. All analyses were performed with R (R.3.6.2.; R Core Team 2018).

3 Results

3.1 Plant size, aboveground biomass, and carbon content

Field height ranged from 0.10 to 2.75 m, whereas root collar diameter ranged from 0.4 to 8.2 cm. Leaf and stem biomass ranged from 0.0004 to 2.31 kg and from 0.0002 to 7.84 kg, respectively. The lowest measured value of total aboveground biomass was 0.0007 kg, whereas the highest was 8.38 kg. We found strong significant associations between field height and leaf biomass (ρ: 0.86, p-value < 0.001), stem biomass (ρ: 0.90, p-value < 0.001), and total aboveground biomass (ρ: 0.90, p-value < 0.001), although the data were highly dispersed in all cases (Figure 6 in Appendix).

The average carbon content in leaves and stems was 46.0 ± 0.02% and 42.6 ± 0.34%, respectively. Leaf carbon dry weight ranged from 0.0002 to 1.06 kg, whereas stem carbon dry weight ranged from 0.0001 to 3.34 kg.

3.2 Calibration of UAV estimates of box height and volume

Box height ($R^2 = 0.96$, $RMSE = 0.0325$, $MBE = 0.00036$, p-value < 0.001, $n = 43$) and box volume ($R^2 = 0.96$, $RMSE = 0.0045$, $MBE = 0.0026$, p-value < 0.001, $n = 43$) showed strong relationships between UAV estimates and laboratory measurements (Figure 7 in Appendix).

3.3 Relationships between UAV estimates with variables measured in the field, aboveground biomass, and carbon stocks

The linear and second-order polynomial regressions between UAV-derived height and field height showed similar determination coefficients and RMSE and AIC

values, but we selected the linear regression as the final model because it had the lowest number of terms (Fig. 2a and Table 1 in Appendix). Moreover, the second-, third-, and fourth-order polynomial regressions as well as the logarithmic regression between UAV-derived height and total aboveground biomass gave very large values of R^2 adjusted and the lowest RMSE and AIC.

We selected the second-order polynomial regression because it exhibited the lowest number of terms (Fig. 2b and Table 2 in Appendix). The second-order polynomial regressions between biovolume with leaf biomass (Fig. 2c and Table 3 in Appendix), stem biomass (Fig. 2d and Table 4 in Appendix), and total aboveground biomass (Fig. 2e and Table 5 in Appendix) and between
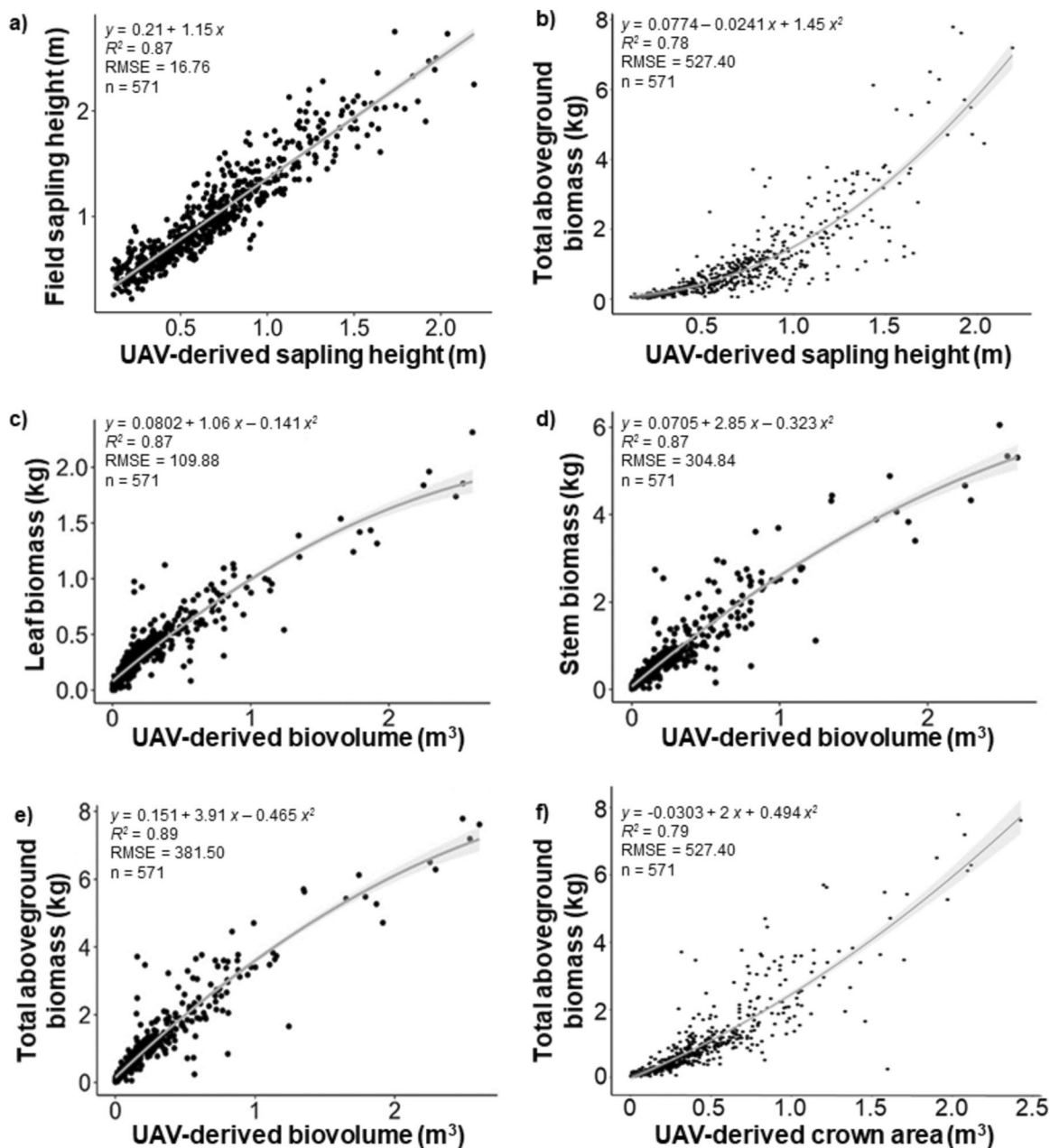

Fig. 2 Linear regression between UAV-derived sapling height (m) and field sapling height (m) (**a**), second-order polynomial regression between UAV-derived sapling height (m) and total aboveground biomass (kg) (**b**), second-order polynomial regression between UAV-derived biovolume (m^3) and leaf biomass (kg) (**c**), second-order polynomial regression between UAV-derived biovolume (m^3) and stem biomass (kg) (**d**), second-order polynomial regression between UAV-derived biovolume (m^3) and total aboveground biomass (kg) (**e**), and second-order polynomial regression between UAV-derived crown area (m^2) and total aboveground biomass (kg) (**f**). RMSE, root-mean-square error

Juan-Ovejero *et al. Annals of Forest Science*   (2023) 80:44

Page 7 of 14

crown area with total aboveground biomass (Fig. 2f and Table 6 in Appendix) yielded the largest determination coefficients and the lowest RMSE and AIC values. The models ultimately selected were as follows:

$$Field\ sapling\ height = 0.21 + 1.15\left(UAV - derived\ sapling\ height\right) \tag{3}$$

$$Total\ aboveground\ biomass = 0.0774 - 0.0241\left(UAV - derived\ sapling\ height\right)$$
$$+ 1.45\left(UAV - derived\ tree\ height\right)^2 \tag{4}$$

$$Leaf\ biomass = 0.0802 + 1.06(UAV - derived\ biovolume)$$
$$- 0.141\left(UAV - derived\ biovolume\right)^2 \tag{5}$$

$$Stem\ biomass = 0.0705 + 2.85(UAV - derived\ biovolume)$$
$$- 0.323\left(UAV - derived\ biovolume\right)^2 \tag{6}$$

$$Total\ aboveground\ biomass = 0.1515 + 3.91(UAV - derived\ biovolume)$$
$$- 0.465\left(UAV - derived\ biovolume\right)^2 \tag{7}$$

$$Total\ aboveground\ biomass = -0.0303 + 2(UAV - derived\ crown\ area)$$
$$+ 0.494\left(UAV - derived\ crown\ size\right)^2 \tag{8}$$

Furthermore, for aboveground carbon stocks, the second-order polynomial regressions between biovolume with leaf carbon dry weight (Fig. 3a and Table 7 in Appendix) and with stem carbon dry weight (Fig. 3b and Table 8 in Appendix) gave the highest R^2 adjusted and the lowest values of RMSE and AIC. The final selected models were of the form as follows:

$$Leaf\ carbon\ dry\ weight = 0.0369 + 0.485(UAV - derived\ biovolume)$$
$$- 0.065(UAV - derived\ biovolume)^2 \tag{9}$$

$$Stem\ carbon\ dry\ weight = 0.03 + 1.22(UAV - derived\ crown\ area)$$
$$- 0.138(UAV - derived\ crown\ area)^2 \tag{10}$$

3.4 Aboveground biomass outputs from field height and UAV-derived height using allometric equations

Estimated aboveground biomass with field height measurements (Fig. 4a, c) and with UAV-derived height (Fig. 4b, d) showed similar fits to real aboveground biomass data. Model 1 for evergreen broadleaf forest species gave $R^2 = 0.66$ using field height measurements 4a) and $R^2 = 0.68$ using UAV-derived height (Fig. 4b). Moreover, model 2 for holm oak showed $R^2 = 0.65$ using field height (Fig. 4c) and $R^2 = 0.68$ for UAV-derived height (Fig. 4d).

4 Discussion

This study shows that 3D point clouds generated from RGB images provide a fast, accurate, and low-cost approach for estimating plant aboveground biomass and carbon stocks in *Quercus ilex* young plantations devoid of litter and understory layers. This is a key issue to solve for the successful integration of forestry activities into carbon markets, which requires regular monitoring and auditing from the early stages of these projects (i.e., every 5 years; REDD 2010). In addition, there has been a continued increase in forest restoration projects in recent years (Mansourian et al. 2021), which further emphasizes the importance of
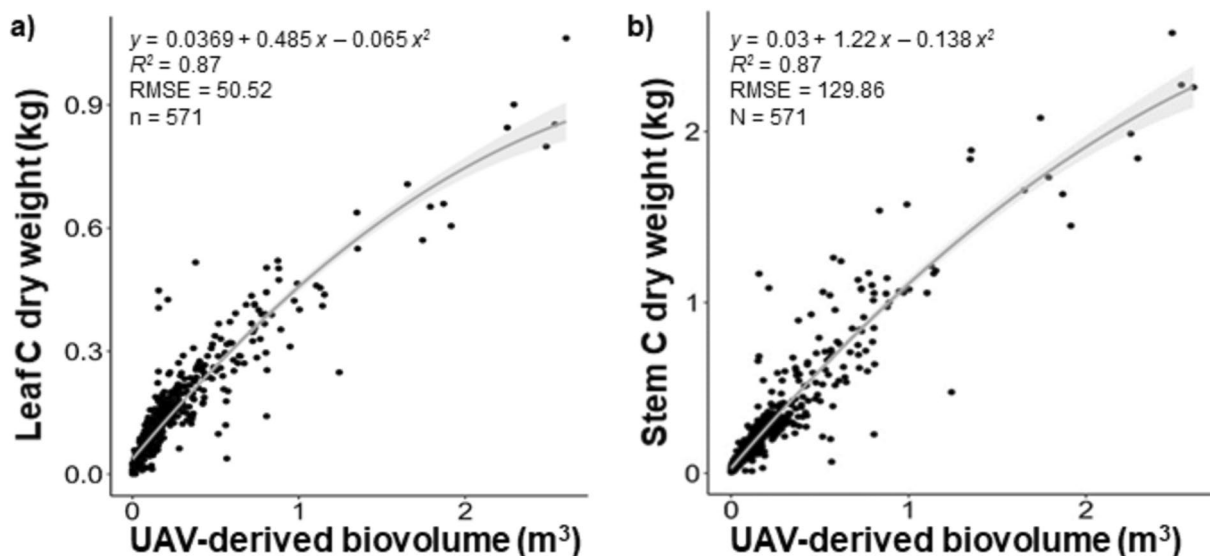

Fig. 3 Second-order polynomial regression between UAV-derived biovolume (m²) and leaf carbon dry weight (kg) (**a**) and second-order polynomial regression between UAV-derived biovolume (m³) and stem carbon dry weight (kg) (**b**). RMSE, root-mean-square error

Juan-Ovejero *et al. Annals of Forest Science*   (2023) 80:44
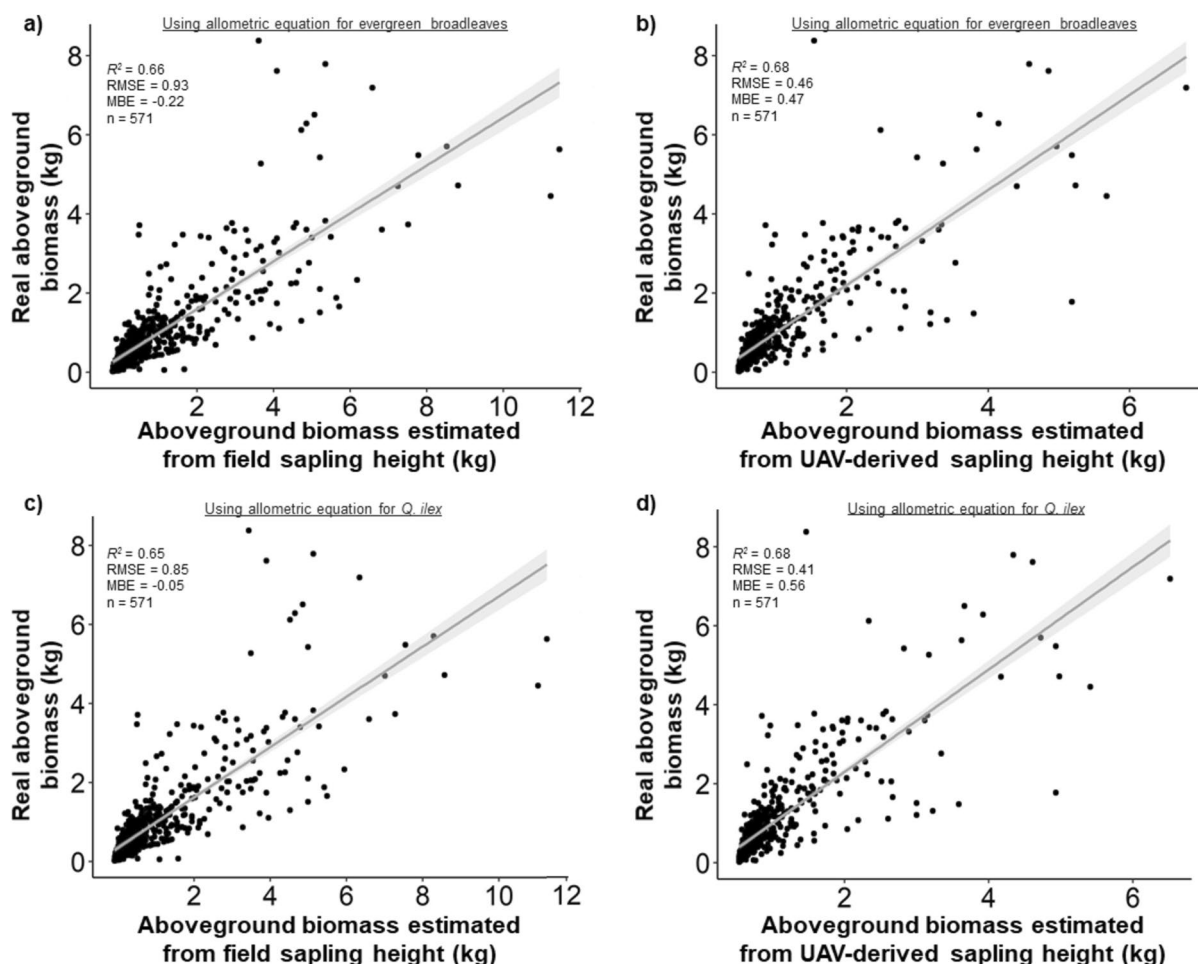
Page 8 of 14

Fig. 4 Linear regressions between aboveground biomass estimated with allometric equations with real aboveground biomass values: using field tree height and model (1) (**a**), using UAV-derived tree height and model (1) (**b**), using field tree height and model (2) (**c**), and using UAV-derived tree height and model (2) (**d**). RMSE, root-mean-square error; MBE, mean bias error

monitoring saplings, especially since information about the growth and carbon uptake capacity of these newly planted trees is scarce (Waring et al. 2020). Our approach may therefore provide a useful, simple, and scalable tool to overcome these challenges, thereby bypassing the need for intensive, time-consuming, and limiting field samplings.

The results indicate that all variables extracted from the high-resolution RGB data showed a significant correlation with field-based measurements, comparable to previous research on small plants (e.g., shrubs; Zhang 2019) and surpassing those for young poplars (Peña et al. 2018). Moreover, we found that the holm oak aboveground biomass and carbon stocks may easily be estimated from the biovolume, a parameter that can be conveniently obtained from drone imagery. Specifically, as reflected by our models, leaf, stem, and total aboveground biomass showed high fits to biovolume. However, these variables cannot be predicted simultaneously with RGB data. In general, our favorable outcomes are obtained despite the heterogeneous crown shape of

holm oaks (Fig. 1b), which often develop lateral branches projected horizontally, making it more challenging to accurately estimate their biomass and carbon sequestration. This suggests that the estimations for trees with a more structured canopy, such as conifers, may be even more precise. Thus, all of this presents the opportunity to develop a novel and efficient method for estimating carbon uptake in young plantations or restorations, regardless of their origin (i.e., natural or human made).

Our approach to estimating aboveground biomass and carbon stocks is powerful and significant not only in terms of accuracy and efficiency but also in terms of cost and time. Field-based methods require the sampling of plant size for any new estimation of carbon stock, which necessitates the mobilization of human resources and the expenditure of days of work. Instead, the approach described here significantly reduces the effort and time required for sampling. Once a correlation is established between the size parameters (e.g., real biomass *versus* drone-estimated

volume), the carbon sequestration monitoring may be done in a matter of hours by a single team of drone operators without the need for additional field sampling. There are also other technologies suitable for estimating plant structures and carbon content. LiDAR, for instance, can provide detailed three-dimensional vertical and horizontal information on canopy structure, resulting in more accurate estimates of plant allometric parameters (Cao et al. 2019; Coops et al. 2007; García et al. 2010; Popescu 2007; Wallace et al. 2016). However, these technologies are still more expensive than RGB cameras (Hummel et al. 2011; McNicol et al. 2021). In addition, the data collected from these technologies are difficult to process, demand heavy operations, and require powerful processing resources (Kumar et al. 2015; Wallace et al. 2016). In summary, our relationships between field and drone data have created a new path for the use of UAV with RGB cameras, and this could be considered a low-cost and time-effective data acquisition alternative that allows to maintain an acceptable spatial and temporal resolution, making it accessible to a wide scope of practitioners and administrations.

Our approach also provides a biomass estimation method that does not require the DBH value, which is a key parameter for traditional field-based biomass allometric equations used in several studies (Correia et al. 2018; Menéndez-Miguélez et al. 2013; Monika et al. 2015; Ruiz-Peinado et al. 2011, 2012). However, the trees in young plantations may be below the height threshold of 130 cm necessary when measuring DBH, particularly in areas where abiotic factors such as drought or temperature limit vigorous growth, as is the case in this study (i.e., Mediterranean-type ecosystems). In fact, only a few studies have developed equations for estimating the biomass and carbon stocks of young trees without accounting for the DBH (Annighöfer et al. 2016; Cotillas et al. 2016; Menéndez-Miguélez et al. 2022). Apart from this, our model regressing UAV-derived sapling height against total aboveground biomass (Fig. 2b) gave a greater fit (R^2: 0.78) to the homologues method proposed by Menéndez-Miguélez et al. (2022) with field sapling height (Fig. 4a, c) and UAV-derived sapling height measurements (Fig. 4b, d), thereby highlighting the effectiveness and usefulness of the approach here proposed.

Although the estimates were highly correlated with aboveground biomass, it is important to mention that the conditions in the study area were particularly favorable for RGB imagery. The success of a drone flight is undeniably influenced by atmospheric conditions, and the precision of our models may not be as accurate as our outcomes have shown if the flight occurs on a day with overcast weather that could reduce the quality of data collected by the onboard sensors (Anderson and Gaston 2013). Moreover, the experimental site was ploughed regularly to remove weeds, and this was also done 1 week before the

drone flight. Saplings were therefore clearly visible and easily detected over the bare surface of the soil. It may be very likely that in other contexts where aboveground carbon stocks need to be estimated, there may be other elements that need to be separated from the trees in the RGB imagery. Our study may therefore not be representative of other "real-world situations," such as artificially or naturally regenerated forests, where litter and understory vegetation cover a high percentage of the ground and may complicate RGB data processing. Thus, more focus should be dedicated to the automatic recognition, separation, and identification of the different shapes and sizes of the various species. Deep learning techniques could be a great solution for such an issue (Egli and Höpke 2020; Ferreira et al. 2020; Fromm et al. 2019; Onishi and Ise 2021; Schiefer et al. 2020), since this will reduce the manual processing and selection of the trees in the RGB data and subsequently increase the efficiency and accuracy of these models. Moreover, it is important to remark that our models were developed with data from only one study site, and this limitation prevents us from extrapolating our results to other holm oak plantations where the aspect and slope of the terrain or the presence of understory could affect the quality of the image or the individual object segmentation. For the scalability of this approach, we need to evaluate the accuracy of the method for species with different growth habits and under other environmental circumstances. In future studies, it would therefore be necessary to perform UAV flights in different mono-specific and mixed forests to address the variability in several factors that may influence the outcomes of our models.

5 Conclusion

The present study shows that RGB imagery acquired with UAV may be a reliable, cost-effective, and scalable approach for the estimation of the aboveground biomass and carbon stocks in young trees. This may be particularly relevant for the monitoring of plantations in the context of the carbon credit markets or the assessment of increasing number of global commitments and initiatives to restore forests (e.g., Castro et al. 2021). Moreover, it is expected that this method will produce even more accurate results for trees that have a more uniform structure (e.g., consistent trunk diameters, well-defined canopies, and a predictable branching pattern). Nevertheless, testing and evaluating the accuracy of the method for species with different growth habits and under other circumstances (e.g., different plant cover) are recommended to assess its potential and powerfulness as well as to create models for different scenarios. Through further research, this approach might be applied for the estimation of aboveground carbon stocks in young forest stands of different tree species and different bioclimatic zones.
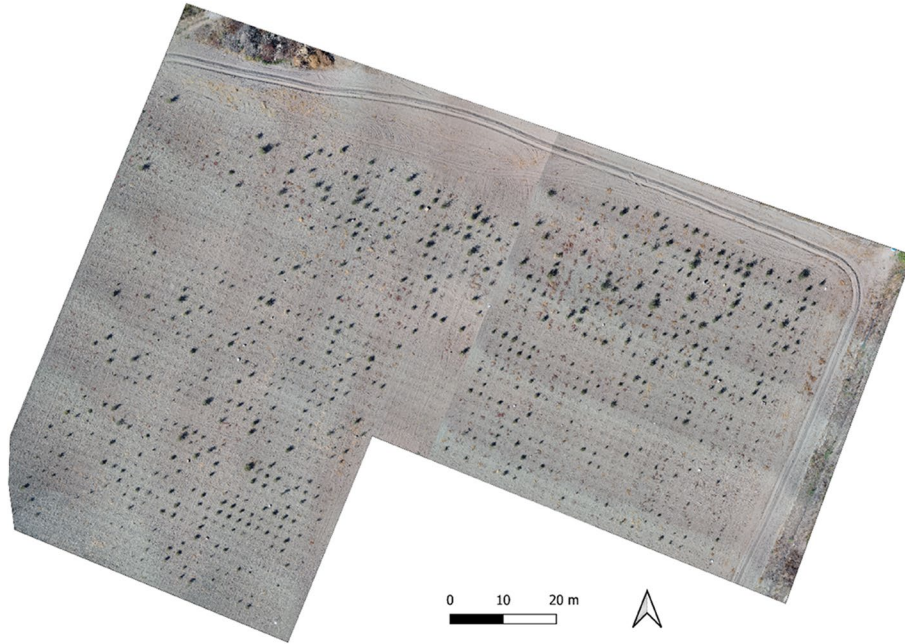
Appendix

Fig. 5 RGB orthomosaic image obtained during the flight campaign performed on September 17, 2021
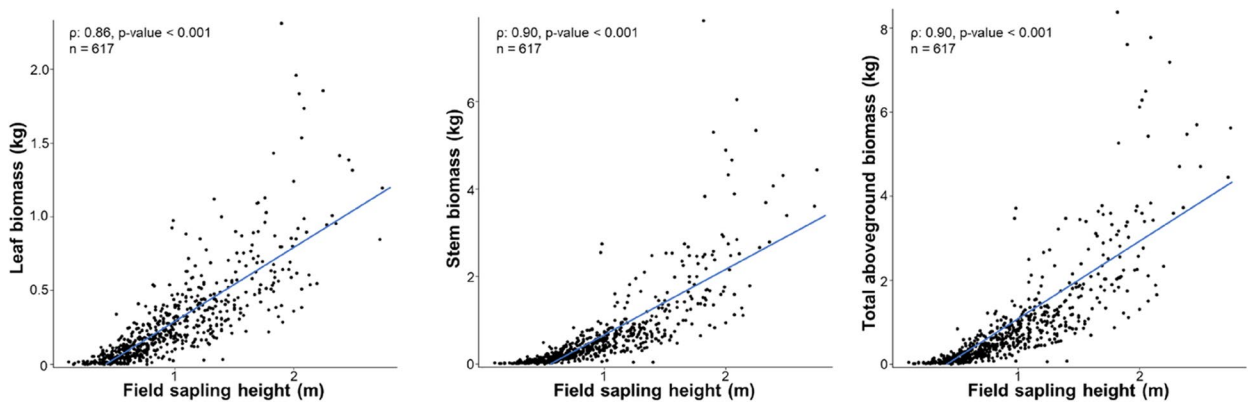

Fig. 6 Scatterplots showing the relationships between field tree height and leaf, stem, and total aboveground biomass
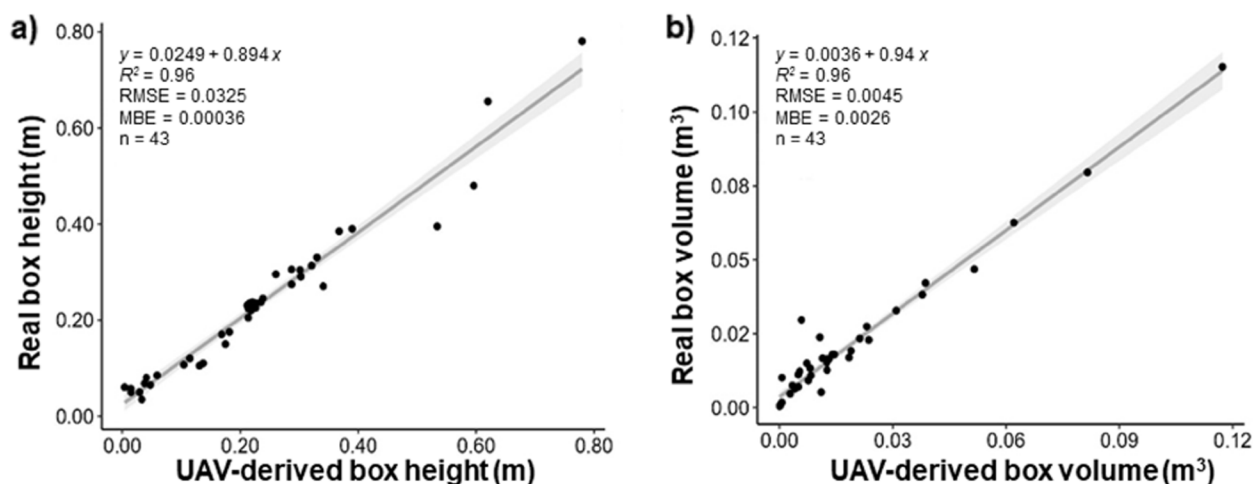
Fig. 7 Linear regressions between UAV-derived box height (m) and real box height (m) (**a**) and between UAV-derived box volume (m³) and real box volume (m³) (**b**). RMSE, root-mean-square error; MBE, mean bias error

Table 1 Regression models between UAV-derived sapling height and field tree height ($n = 571$)

Model	R^2 adjusted	*p*-value	RMSE	AIC
Lineal	0.87	< 0.001	16.76	4818.00
Second-order polynomial regression	0.87	< 0.001	16.74	4817.60
Third-order polynomial regression	0.88	< 0.001	16.69	4814.69
Fourth-order polynomial regression	0.88	< 0.001	16.66	4812.25
Logarithmic regression	0.76	< 0.001	23.01	5178.29
Inverse exponential regression	0.79	< 0.001	21.80	5116.75

RMSE root-mean-square error; *AIC* Akaike information criterion

Table 3 Regression models between UAV-derived biovolume and leaf biomass ($n = 571$)

Model	R^2 adjusted	*p*-value	RMSE	AIC
Lineal	0.85	< 0.001	117.16	7027.28
Second-order polynomial regression	0.87	< 0.001	109.88	6955.36
Third-order polynomial regression	0.86	< 0.001	112.51	6982.24
Fourth-order polynomial regression	0.86	< 0.001	113.85	6995.78
Logarithmic regression	0.58	< 0.001	199.30	7630.84
Inverse exponential regression	0.62	< 0.001	187.32	7560.39

RMSE, root-mean-square error; *AIC*, Akaike information criterion

Table 2 Regression models between UAV-derived sapling height and total aboveground biomass ($n = 571$)

Model	R^2 adjusted	*p*-value	RMSE	AIC
Lineal	0.71	< 0.001	622.50	8924.65
Second-order polynomial regression	0.78	< 0.001	547.03	8778.81
Third-order polynomial regression	0.78	< 0.001	546.12	8776.92
Fourth-order polynomial regression	0.77	< 0.001	549.62	8784.19
Logarithmic regression	0.51	< 0.001	809.48	9223.02
Inverse exponential regression	0.78	< 0.001	546.00	8775.69

RMSE, root-mean-square error; *AIC*, Akaike information criterion

Table 4 Regression models between UAV-derived biovolume and stem biomass ($n = 571$)

Model	R^2 adjusted	*p*-value	RMSE	AIC
Lineal	0.86	< 0.001	318.61	8163.78
Second-order polynomial regression	0.87	< 0.001	304.83	8114.53
Third-order polynomial regression	0.87	< 0.001	306.25	8119.84
Fourth-order polynomial regression	0.87	< 0.001	307.76	8125.42
Logarithmic regression	0.49	< 0.001	616.53	8913.69
Inverse exponential regression	0.64	< 0.001	518.88	8717.82

RMSE, root-mean-square error; *AIC*, Akaike information criterion

Juan-Ovejero *et al. Annals of Forest Science*   (2023) 80:44

Page 12 of 14

Table 5 Regression models between UAV-derived biovolume and total aboveground biomass (n = 571)

Model	R^2 adjusted	*p*-value	RMSE	AIC
Lineal	0.88	< 0.001	404.21	8434.10
Second-order polynomial regression	0.89	< 0.001	381.50	8369.42
Third-order polynomial regression	0.89	< 0.001	385.75	8381.99
Fourth-order polynomial regression	0.89	< 0.001	388.87	8391.15
Logarithmic regression	0.52	< 0.001	800.69	9210.61
Inverse exponential regression	0.65	< 0.001	687.17	9036.92

RMSE, root-mean-square error; *AIC*, Akaike information criterion

Table 8 Regression models between UAV-derived biovolume and stem carbon dry weight (*n* = 571)

Model	R^2 adjusted	*p*-value	RMSE	AIC
Lineal	0.86	< 0.001	135.73	7194.41
Second-order polynomial regression	0.87	< 0.001	129.86	7145.16
Third-order polynomial regression	0.87	< 0.001	130.46	7150.47
Fourth-order polynomial regression	0.87	< 0.001	131.11	7156.05
Logarithmic regression	0.49	< 0.001	262.64	7944.33
Inverse exponential regression	0.64	< 0.001	221.04	7748.45

RMSE, root-mean-square error; *AIC*, Akaike information criterion

Table 6 Regression models between UAV-derived crown area and total aboveground biomass (*n* = 571)

Model	R^2 adjusted	*p*-value	RMSE	AIC
Lineal	0.78	< 0.001	541.40	8766.07
Second-order polynomial regression	0.79	< 0.001	527.41	8737.33
Third-order polynomial regression	0.79	< 0.001	527.49	8737.51
Fourth-order polynomial regression	0.79	< 0.001	527.81	8738.20
Logarithmic regression	0.43	< 0.001	874.61	9310.92
Inverse exponential regression	0.74	< 0.001	589.95	8863.63

RMSE, root-mean-square error; *AIC*, Akaike information criterion

Table 7 Regression models between UAV-derived biovolume and leaf carbon dry weight (*n* = 571)

Model	R^2 adjusted	*p*-value	RMSE	AIC
Lineal	0.85	< 0.001	53.87	6144.65
Second-order polynomial regression	0.87	< 0.001	50.52	6072.73
Third-order polynomial regression	0.86	< 0.001	51.73	6099.61
Fourth-order polynomial regression	0.86	< 0.001	52.35	6113.15
Logarithmic regression	0.58	< 0.001	91.64	6748.21
Inverse exponential regression	0.62	< 0.001	86.13	6677.76

RMSE, root-mean-square error; *AIC*, Akaike information criterion

Code availability
The custom code generated during and/or analyzed during the current study is available from the corresponding author on reasonable request.

Authors' contributions
Data curation, RJO and MPRM. Formal analysis, RJO, AE, and CJN. Visualization, RJO, AE, and CJN. Writing—original draft, RJO, AE, and JC. Writing—review and editing, MNJ, FBN, and DAS. Conceptualization, DAS, FBN and JC. Methodology, DAS, FBN and JC. Funding acquistion, DAS, FBN and JC. All authors read and approved the final manuscript.

Availability of data and materials
The datasets generated and analyzed during the current study are available in the Medeley Data repository (https://data.mendeley.com/datasets/nxnsrsnnnw/1). Juan-Ovejero, Raquel; Elghouat, Akram; Navarro, Carlos J.; Reyes-Martín, Marino P.; Jiménez, M. Noelia; Navarro Reyes, Francisco; Alcaraz-Segura, Domingo; and Castro, Jorge (2023), "Estimation of aboveground biomass and carbon stocks of tree saplings using UAV-derived RGB imagery - DATASET," Mendeley Data, V1, https://doi.org/10.17632/nxnsrsnnnw.1.

Declarations

Ethics approval and consent to participate
Not applicable

Consent for publication
All authors gave their informed consent to this publication and its content.

Competing interests
The authors declare that they have no competing interests.

Juan-Ovejero *et al. Annals of Forest Science*   (2023) 80:44

Page 13 of 14

Author details

[1]Department of Life Sciences, Centre for Functional Ecology, University of Coimbra, 3000-456 Coimbra, Portugal. [2]Department of Ecology and Animal Biology, University of Vigo, 36310 Vigo, Spain. [3]Department of Ecology, University of Granada, 18071 Granada, Spain. [4]iEcolab, Interuniversity Institute for Earth System Research (IISTA), University of Granada, 18006 Granada, Spain. [5]2GRNT Laboratory (Geosciences, Geotourism, Natural Hazards, and Remote Sensing), Department of Geology, Faculty of Sciences Semlalia, Cadi Ayyad University, Marrakech, Morocco. [6]Department of Botany, University of Granada, 18071 Granada, Spain. [7]Area of Natural and Forest Resources, Institute of Agricultural Research and Training (IFAPA Centro Camino de Purchil), Government of Andalusia, 18004 Granada, Spain. [8]Andalusian Center for the Assessment and Monitoring of Global Change (CAESCG), University of Almería, 04120 Almería, Spain.

References

Abdullah MM, Al-Ali ZM, Abdullah MT, Srinivasan S, Assi AT, Al Atiqi S (2021) Investigating the applicability of UAVs in characterizing desert shrub biomass and developing biological indicators for the selection of suitable revegetation sites. J Environ Manag 288:112416. https://doi.org/10.1016/j.jenvman.2021.112416

Alivernini A, Barbati A, Merlini P, Carbone F, Corona P (2016) New forests and Kyoto Protocol carbon accounting: a case study in Central Italy. Agric Ecosyst Environ 15:58–65. https://doi.org/10.1016/j.agee.2015.11.006

Anderson K, Gaston KJ (2013) Lightweight unmanned aerial vehicles will revolutionize spatial ecology. Front Ecol Environ 11(3):138–146. https://doi.org/10.1890/120150

Annighöfer P, Ameztegui A, Ammer C, Balandier P, Bartsch N, Bolte A et al (2016) Species-specific and generic biomass equations for seedlings and saplings of European tree species. Eur J For Res 135:313–329. https://doi.org./10.1007/s10342-016-0937-z

Bastin JF, Finegold Y, Garcia C, Mollicone D, Rezende M, Routh D, Zohner CM, Crowther TW (2019) The global tree restoration potential. Science 365:76–79. https://doi.org/10.1126/science.aax0848

Bellassen V, Viovy N, Luyssaert S, le Maire G, Schelhaas MJ, Ciais P (2011) Reconstruction and attribution of the carbon sink of European forests between 1950 and 2000. Glob Chang Biol 17(11):3274–3292. https://doi.org/10.1111/J.1365-2486.2011.02476.X

Cao L, Liu H, Fu X, Zhang Z, Shen X, Ruan H (2019) Comparison of UAV LiDAR and digital aerial photogrammetry point clouds for estimating forest structural attributes in subtropical planted forests. Forests 10(2):145. https://doi.org/10.3390/f10020145

Castro J, Morales-Rueda F, Navarro FB, Löf M, Vacchiano G, Alcaraz-Segura D (2021) Precision restoration: a necessary approach to foster forest recovery in the 21st century. Restor Ecol 29(7):e13421. https://doi.org/10.1111/rec.13421

Coops NC, Hilker T, Wulder MA, St-Onge B, Newnham G, Siggins A, Trofymow JA (2007) Estimating canopy structure of Douglas-fir forest stands from discrete-return LiDAR. Trees 21:295–310. https://doi.org/10.1007/s00468-006-0119-6

Correia AC, Faias SP, Ruiz-Peinado R, Chianucci F, Cutini A, Fontes L, Manetti MC, Montero G, Soares P, Tomé M (2018) Generalized biomass equations for stone pine (Pinus pinea L.) across the Mediterranean Basin. For Ecol Manag 429:425–436. https://doi.org/10.1016/j.foreco.2018.07.037

Cotillas M, Espelta JM, Sánchez-Costa E, Sabaté S (2016) Aboveground and belowground biomass allocation patterns in two Mediterranean oaks with contrasting leaf habit: an insight into carbon stock in young oak coppices. Eur J For Res 135:243–252. https://doi.org/10.1007/s10342-015-0932-9

Edson C, Wing MG (2011) Airborne light detection and ranging (LiDAR) for individual tree stem location, height, and biomass measurements. Remote Sens 3(11):2494–2528. https://doi.org/10.3390/rs3112494

Egli S, Höpke M (2020) CNN-based tree species classification using high resolution RGB image data from automated UAV observations. Remote Sens 12(23):3892. https://doi.org/10.3390/rs12233892

Ferreira MP, de Almeida DRA, de Almeida PD, Minervino JBS, Veras HFP, Formighieri A et al (2020) Individual tree detection and species classification of Amazonian palms using UAV images and deep learning. For Ecol Manag 475:118397. https://doi.org/10.1016/j.foreco.2020.118397

Forrester DI, Tachauer IHH, Annighoefer P, Barbeito I, Pretzsch H, Ruiz-Peinado R, Stark H, Vacchiano G, Zlatnov T, Chakraborty T, Saha S, Sileshi GW (2017) Generalized biomass and leaf area allometric equations for European tree species incorporating stand structure, tree age and climate. For Ecol Manag 396:160–175. https://doi.org/10.1016/j.foreco.2017.04.011

Fromm M, Schubert M, Castilla G, Linke J, McDermid G (2019) Automated detection of conifer seedlings in drone imagery using convolutional neural networks. Remote Sens 11(21):2585. https://doi.org/10.3390/rs11212585

Fuss S, Canadell JG, Ciais P, Jackson RB, Jones CD, Lyngfelt A, Van Vuuren DP (2020) Moving toward net-zero emissions requires new alliances for carbon dioxide removal. One Earth 3:145–149. https://doi.org/10.1016/j.oneear.2020.08.002

García M, Riano D, Chuvieco E, Danson M (2010) Estimating biomass carbon stocks for a Mediterranean forest in Central Spain using LiDAR height and intensity data. Remote Sens Environ 114:816–830. https://doi.org/10.1016/j.rse.2009.11.021

Hall RJ, Skakun RS, Arsenault EJ, Case BS (2006) Modeling forest stand structure attributes using Landsat ETM+ data: application to mapping of aboveground biomass and stand volume. For Ecol Manag 225(1-3):378–390

Hansen J, Sato M, Kharecha P, von Schuckmann K, Beerling DJ, Cao J, Marcott S, Masson-Delmotte V, Prather MJ, Rohling EJ, Shakun J, Smith P, Lacis A, Russell G, Ruedy R (2017) Young people's burden: requirement of negative CO_2 emissions. Earth Syst Dyn 8(3):577–616. https://doi.org/10.5194/ESD-8-577-2017

Hu Y, Zhang Q, Hu S, Xiao G, Chen X, Wang J, Qi Y, Zhang L, Han L (2022) Research progress and prospects of ecosystem carbon sequestration under climate change (1992–2022). Ecol Indic 145:109656. https://doi.org/10.1016/J.ECOLIND.2022.109656

Hummel S, Hudak AT, Uebler EH, Falkowski MJ, Megown KA (2011) A comparison of accuracy and cost of LiDAR versus stand exam data for landscape management on the Malheur National Forest. J For 109(5):267–273. https://doi.org/10.1093/jof/109.5.267

IPCC (2022) Impacts, adaptation and vulnerability. Contribution of Working Group II to the Sixth Assessment Report of the Intergovernmental Panel on Climate Change. Cambridge University Press, Cambridge, UK

Juan-Ovejero R, Elghouat A, Navarro C J, Reyes-Martín M P, Jiménez M N, Navarro Reyes F B, Alcaraz-Segura D, Castro J (2023) Estimation of aboveground biomass and carbon stocks of tree saplings using UAV-derived RGB imagery. [Dataset] Mendeley Data, V1. https://doi.org/10.17632/nxnsrsnnnw.1

Keith H, Vardon M, Obst C, Young V, Houghton RA, Mackey B (2021) Evaluating nature-based solutions for climate mitigation and conservation requires comprehensive carbon accounting. Sci Total Environ 769:144341. https://doi.org/10.1016/J.SCITOTENV.2020.144341

Kumar L, Sinha P, Taylor S, Alqurashi AF (2015) Review of the use of remote sensing for biomass estimation to support renewable energy generation. J Appl Remote Sens 9(1):097696. https://doi.org/10.1117/1.JRS.9.097696

Lacis AA, Schmidt GA, Rind D, Ruedy RA (2010) Atmospheric CO_2: principal control knob governing Earth's temperature. Science 330(6002):356–359. https://doi.org/10.1126/science.1190653

Lewis SL, Wheeler CE, Mitchard ETA, Koch A (2019) Restoring natural forests is the best way to remove atmospheric carbon. Nature 568(7750):25–28. https://doi.org/10.1038/d41586-019-01026-8

Li Y, Li M, Li C, Liu Z (2020) Forest aboveground biomass estimation using Landsat 8 and Sentinel-1A data with machine learning algorithms. Sci Rep 10:9952. https://doi.org/10.1038/s41598-020-67024-3

Luo S, Wang C, Xi X, Pan F, Peng D, Zou J et al (2017) Fusion of airborne LiDAR data and hyperspectral imagery for aboveground and belowground forest biomass estimation. Ecol Indic 73:378–387. https://doi.org/10.1016/j.ecolind.2016.10.001

Lussem U, Bolten A, Menne J, Gnyp ML, Schellberg J, Bareth G (2019) Estimating biomass in temperate grassland with high resolution canopy surface models from UAV-based RGB images and vegetation indices. J Appl Remote Sens 13(3):034525. https://doi.org/10.1117/1.JRS.13.034525

Mansourian S, Berrahmouni N, Blaser J, Dudley N, Maginnis S, Mumba M, Vallauri D (2021) Reflecting on twenty years of forest landscape restoration. Restor Ecol 29:e13441. https://doi.org/10.1111/rec.13441

McCann JA, Keith DA, Kingsford RT (2022) Measuring plant biomass remotely using drones in arid landscapes. Ecol Evol 12(5):e8891. https://doi.org/10.1002/ece3.8891

McNicol IM, Mitchard ET, Aquino C, Burt A, Carstairs H, Dass C et al (2021) To what extent can UAV photogrammetry replicate UAV LiDAR to determine forest structure? A test in two contrasting tropical forests. Journal of Geophysical Research. Biogeosciences 126(12):e2021JG006586. https://doi.org/10.1029/2021JG006586

Menéndez-Miguélez M, Calama R, Del Río M, Madrigal G, López-Senespleda E, Pardos M, Ruiz-Peinado R (2022) Species-specific and generalized biomass models for estimating carbon stocks of young reforestations. Biomass Bioenergy 161:106453. https://doi.org/10.1016/j.biombioe.2022.106453

Menéndez-Miguélez M, Canga E, Barrio-Anta M, Majada J, Álvarez-Álvarez P (2013) A three level system for estimating the biomass of Castanea sativa Mill. coppice stands in North-West Spain. For Ecol Manag 291:417–426. https://doi.org/10.1016/j.foreco.2012.11.040

Menéndez-Miguélez M, Ruiz-Peinado R, Del Río M, Calama R (2021) Improving tree biomass models through crown ratio patterns and incomplete data sources. Eur J For Res 140:675–689. https://doi.org/10.1007/s10342-021-01354-3

Messinger M, Asner GP, Silman M (2016) Rapid assessments of Amazon forest structure and biomass using small unmanned aerial systems. Remote Sens 8:615. https://doi.org/10.3390/rs8080615

Monika V, Daniel Z, Tomáš Č, Vít Š (2015) Models for predicting aboveground biomass of European beech (Fagus sylvatica L.) in the Czech Republic. J For Sci 61(2):45–54. https://doi.org/10.17221/100/2014-JFS

Murfitt SL, Allan BM, Bellgrove A, Rattray A, Young MA, Ierodiaconou D (2017) Applications of unmanned aerial vehicles in intertidal reef monitoring. Sci Rep 7:10259. https://doi.org/10.1038/s41598-017-10818-9

Navarro A, Young M, Allan B, Carnell P, Macreadie P, Ierodiaconou D (2020) The application of unmanned aerial vehicles (UAVs) to estimate above-ground biomass of mangrove ecosystems. Remote Sens Environ 242:111747. https://doi.org/10.1016/j.rse.2020.111747

Onishi M, Ise T (2021) Explainable identification and mapping of trees using UAV RGB image and deep learning. Sci Rep 11(1):903. https://doi.org/10.1038/s41598-020-79653-9

Pan C, Shrestha A, Innes JL, Zhou G, Li N, Li J, Wang G (2022) Key challenges and approaches to addressing barriers in forest carbon offset projects. J For Res 33:1109–1122. https://doi.org/10.1007/s11676-022-01488-z

Pan Y, Birdsey RA, Fang J, Houghton R, Kauppi PE, Kurz WA et al (2011) A large and persistent carbon sink in the world's forests. Science 333(6045):988–993. https://doi.org/10.1126/science.1201609

Peña JM, de Castro AI, Torres-Sánchez J, Andújar D, San Martín C, Dorado J, Fernández-Quintanilla C, López-Granados F (2018) Estimating tree height and biomass of a poplar plantation with image-based UAV technology. AIMS Agric Food 3(3):313–326. https://doi.org/10.3934/agrfood.2018.3.172

Popescu SC (2007) Estimating biomass of individual pine trees using airborne LiDAR. Biomass Bioenergy 31:646–655. https://doi.org/10.1016/j.biombioe.2007.06.022

R Core Team (2018) R: a language and environment for statistical computing. R Foundation for Statistical Computing, Vienna, Austria

REDD Methodological Module 2010. Estimation of carbon stocks and changes in the above- and below-ground biomass pools – CP-AB. Version - May 2010; Available at https://americancarbonregistry.org/carbon-accounting/old/carbon-accounting/CP-AB.pdf

Ruiz-Peinado R, del Rio M, Montero G (2011) New models for estimating the carbon sink capacity of Spanish softwood species. For Sys 20(1):176–188. https://doi.org/10.5424/fs/2011201-11643

Ruiz-Peinado R, Montero G, Del Río M (2012) Biomass models to estimate carbon stocks for hardwood tree species. For Syst 21(1):42–52. https://doi.org/10.5424/fs/2112211-02193

Ruwaimana M, Satyanarayana B, Otero V, Muslim AM, Muhammad Syafiq A, Ibrahim S, Raymaekers D, Koedam N, Dahdouh-Guebas F (2018) The advantages of using drones over space-borne imagery in the mapping of mangrove forests. PLoS One 13:1–22. https://doi.org/10.1371/journal.pone.0200288

Schiefer F, Kattenborn T, Frick A, Frey J, Schall P, Koch B, Schmidtlein S (2020) Mapping forest tree species in high resolution UAV-based RGB-imagery by means of convolutional neural networks. ISPRS J Photogramm Remote Sens 170:205–215. https://doi.org/10.1016/j.isprsjprs.2020.10.015

Schoene D (2003) Terms and pathways for assessing and reporting forest carbon change. XII World Forestry Congress, Quebec, Canada https://www.fao.org/3/XII/0865-B1.htm

Sullivan MJ, Lewis SL, Hubau W, Qie L, Baker TR, Banin LF et al (2018) Field methods for sampling tree height for tropical forest biomass estimation. Methods Ecol Evol 9(5):1179–1189. https://doi.org/10.1111/2041-210X.12962

Turner-Skoff JB, Cavender N (2019) The benefits of trees for livable and sustainable communities. Plants People Planet 1(4):323–335. https://doi.org/10.1002/PPP3.39

Vacchiano G, Berretti R, Romano R, Motta R (2018) Voluntary carbon credits from improved forest management: policy guidelines and case study. iForest-Biogeosciences and Forestry 11:1–10. https://doi.org/10.3832/ifor2431-010

van der Gaast W, Sikkema R, Vohrer M (2018) The contribution of forest carbon credit projects to addressing the climate change challenge. Clim Pol 18(1):42–48. https://doi.org/10.1080/14693062.2016.1242056

Velázquez E, Martínez-Jaraíz C, Wheeler C, Mitchard ETA, Bravo F (2022) Forest expansion in abandoned agricultural lands has limited effect to offset carbon emissions from Central-North Spain. Reg Environ Chang 22:132. https://doi.org/10.1007/s10113-022-01978-0

Vorster AG, Evangelista PH, Stovall AEL, Ex S (2020) Variability and uncertainty in forest biomass estimates from the tree to landscape scale: the role of allometric equations. Carbon Balance Manag 15:8. https://doi.org/10.1186/s13021-020-00143-6

Wallace L, Lucieer A, Malenovský Z, Turner D, Vopěnka P (2016) Assessment of forest structure using two UAV techniques: a comparison of airborne laser scanning and structure from motion (SfM) point clouds. Forests 7(3):62. https://doi.org/10.3390/f7030062

Waring B, Neumann M, Prentice IC, Adams M, Smith P, Siegert M (2020) Forests and decarbonization–roles of natural and planted forests. Frontiers in Forests and Global. Change 3:58. https://doi.org/10.3389/ffgc.2020.00058

Weiskittel AR, MacFarlane DW, Radtke PJ, Affleck DLR, Temesgen H, Woodall CW, Westfall JA, Coulston JW (2015) A call to improve methods for estimating tree biomass for regional and national assessments. J For 113(4):414–424. https://doi.org/10.5849/JOF.14-091

Yang H, Ciais P, Santoro M, Huang Y, Li W, Wang Y, Bastos A, Goll D, Arneth A, Anthoni P, Arora VK, Friedlingstein P, Harverd V, Joetzjer E, Kautz M, Lienert S, Nabel JEMS, O'Sullivan M, Sitch S et al (2020) Comparison of forest above-ground biomass from dynamic global vegetation models with spatially explicit remotely sensed observation-based estimates. Glob Chang Biol 26(7):3997–4012. https://doi.org/10.1111/GCB.15117

Zhang X (2019) Quick aboveground carbon stock estimation of densely planted shrubs by using point cloud derived from unmanned aerial vehicle. Remote Sens 11(24):2914. https://doi.org/10.3390/rs11242914

Publisher's note